Research Article | Vol. 26, No. 10 | 14 May 2018 | OPTICS EXPRESS A398
Optics EXPRESS

Full modeling and experimental validation of cylindrical holographic lenses recorded in Bayfol HX photopolymer and partly operating in the transition regime for solar concentration

JULIA MARÍN-SÁEZ,[1] JESÚS ATENCIA,[2,*] DANIEL CHEMISANA,[1] AND MARÍA-VICTORIA COLLADOS[2]

[1]*Applied Physics Section of the Environmental Science Department, Polytechnic School, University of Lleida, Jaume II 69, 25001 Lleida, Spain*
[2]*Applied Physics Department, Aragon Institute of Engineering Research (I3A), Faculty of Science, University of Zaragoza, Pedro Cerbuna 12, 50009 Zaragoza, Spain*
**atencia@unizar.es*

Abstract: Concentrating photovoltaics for building integration can be successfully carried out with Holographic Optical Elements (HOEs) because of their behavior analogous to refractive optical elements and their tuning ability to the spectral range that the photovoltaic (PV) cell is sensitive to. That way, concentration of spectral ranges that would cause overheating of the cell is avoided. Volume HOEs are usually chosen because they provide high efficiencies. However, their chromatic selectivity is also very high, and only a small part of the desired spectral range reaches the PV cell. A novel approach is theoretically and experimentally explored to overcome this problem: the use of HOEs operating in the transition regime, which yield lower chromatic selectivity while keeping rather high efficiencies. A model that considers the recording material's response, by determining the index modulation reached for each spatial frequency and exposure dosage, has been developed. It has been validated with experimental measurements of three cylindrical holographic lenses with different spatial frequency ranges recorded in Bayfol HX photopolymer. Simulations of systems comprising two lenses and a mono-c Si PV cell are carried out with the standard AM 1.5D solar spectrum. Promising results are obtained when using the system with lower spatial frequencies lenses: a total current intensity equal to 3.72 times the one that would be reached without the concentrator.

OCIS codes: (090.0090) Holography; (090.1970) Diffractive optics; (090.2890) Holographic optical elements; (350.6050) Solar energy; (050.1965) Diffractive lenses.

References and links

1. D. Chemisana, "Building integrated concentrating photovoltaics: A review," Renew. Sustain. Energy Rev. **15**(1), 603–611 (2011).
2. H. Baig, N. Sarmah, D. Chemisana, J. Rosell, and T. K. Mallick, "Enhancing performance of a linear dielectric based concentrating photovoltaic system using a reflective film along the edge," Energy **73**, 177–191 (2014).
3. D. Chemisana and M. Ibáñez, "Linear Fresnel concentrators for building integrated applications," Energy Convers. Manage. **51**(7), 1476–1480 (2010).
4. G. Li, G. Pei, M. Yang, J. Ji, and Y. Su, "Optical evaluation of a novel static incorporated compound parabolic concentrator with photovoltaic/thermal system and preliminary experiment," Energy Convers. Manage. **85**, 204–211 (2014).
5. N. Yamada, K. Kanno, K. Hayashi, and T. Tokimitsu, "Performance of see-through prism CPV module for window integrated photovoltaics," Opt. Express **19**(S4 Suppl 4), A649–A656 (2011).
6. M. V. Collados, D. Chemisana, and J. Atencia, "Holographic solar energy systems: The role of optical elements," Renew. Sustain. Energy Rev. **59**, 130–140 (2016).
7. American Society for Testing and Materials, "Standard tables for reference solar spectral irradiances: direct normal and hemispherical on 37° tilted surface," in *Book of Standards Volume: 14.04* (2004).
8. R. K. Kostuk and G. Rosenberg, "Analysis and design of holographic solar concentrators," Proc. SPIE **7043**,

#319983 https://doi.org/10.1364/OE.26.00A398
Journal © 2018 Received 18 Jan 2018; revised 16 Mar 2018; accepted 17 Mar 2018; published 28 Mar 2018

Optics EXPRESS

70430I (2008).
9. J. M. Castro, D. Zhang, B. Myer, and R. K. Kostuk, "Energy collection efficiency of holographic planar solar concentrators," Appl. Opt. **49**(5), 858–870 (2010).
10. H. Akbari, I. Naydenova, and S. Martin, "Using acrylamide-based photopolymers for fabrication of holographic optical elements in solar energy applications," Appl. Opt. **53**(7), 1343–1353 (2014).
11. J. E. Ludman, J. Riccobono, N. O. Reinhand, I. V. Semenova, J. Martín, W. Tai, X. Li, and G. Syphers, "Holographic solar concentrator for terrestrial photovoltaics," in *Proceedings of the 24th IEEE Photovoltaic Specialists Conference* (1994), pp. 1208–1211.
12. J. E. Ludman, J. Riccobono, I. V. Semenova, N. O. Reinhand, W. Tai, X. Li, G. Syphers, E. Rallis, G. Sliker, and J. Martín, "The optimization of a holographic system for solar power generation," Sol. Energy **60**(1), 1–9 (1997).
13. K. Froehlich, E. U. Wagemann, H. Schulat, H. Schuette, and C. G. Stojanoff, "Fabrication and test of a holographic concentrator for two-color PV operation," Proc. SPIE **2255**, 812–821 (1994).
14. D. Zhang, M. Gordon, J. M. Russo, S. Vorndran, and R. K. Kostuk, "Spectrum-splitting photovoltaic system using transmission holographic lenses," J. Photonics Energy **3**(1), 34597 (2013).
15. S. Vorndran, J. M. Russo, Y. Wu, M. Gordon, and R. Kostuk, "Holographic diffraction-through-aperture spectrum splitting for increased hybrid solar energy conversion efficiency," Int. J. Energy Res. **39**(3), 326–335 (2015).
16. H. Akbari, I. Naydenova, H. Ahmed, S. McCormack, and S. Martin, "Development and testing of low spatial frequency holographic concentrator elements for collection of solar energy," Sol. Energy **155**, 103–109 (2017).
17. D. Chemisana, M. V. Collados, M. Quintanilla, and J. Atencia, "Holographic lenses for building integrated concentrating photovoltaics," Appl. Energy **110**, 227–235 (2013).
18. P. Bañares-Palacios, S. Álvarez-Álvarez, J. Marín-Sáez, M.-V. Collados, D. Chemisana, and J. Atencia, "Broadband behavior of transmission volume holographic optical elements for solar concentration," Opt. Express **23**(11), A671–A681 (2015).
19. J. Marín-Sáez, D. Chemisana, Á. Moreno, A. Riverola, J. Atencia, and M.-V. Collados, "Energy Simulation of a Holographic PVT Concentrating System for Building Integration Applications," Energies **9**(8), 577 (2016).
20. M. G. Moharam, T. K. Gaylord, and R. Magnusson, "Criteria for Bragg regime diffraction by phase gratings," Opt. Commun. **32**(1), 14–18 (1980).
21. M. G. Moharam, T. K. Gaylord, and R. Magnusson, "Criteria for Raman-Nath regime diffraction by phase gratings," Opt. Commun. **32**(1), 19–23 (1980).
22. W. H. Bloss, M. Griesinger, and E. R. Reinhardt, "Dispersive concentrating systems based on transmission phase holograms for solar applications," Appl. Opt. **21**(20), 3739–3742 (1982).
23. C. Bainier, C. Hernandez, and D. Courjon, "Solar concentrating systems using holographic lenses," Solar Wind Technol. **5**(4), 395–404 (1988).
24. G. B. Ingersoll and J. R. Leger, "Optimization of multi-grating volume holographic spectrum splitters for photovoltaic applications," Appl. Opt. **55**(20), 5399–5407 (2016).
25. A. Villamarín, J. Atencia, M. V. Collados, and M. Quintanilla, "Characterization of transmission volume holographic gratings recorded in Slavich PFG04 dichromated gelatin plates," Appl. Opt. **48**(22), 4348–4353 (2009).
26. R. Syms, *Practical Volume Holography* (Oxford University Press, 1990).
27. W. R. Klein and B. D. Cook, "Unified Approach to Ultrasonic Light Diffraction," IEEE Trans. Sonics Ultrason. **14**(3), 123–134 (1967).
28. H. Kogelnik, "Coupled wave theory for thick hologram gratings," Bell Syst. Tech. J. **48**(9), 2909–2947 (1969).
29. F.-K. Bruder, T. Fäcke, and T. Rölle, "The Chemistry and Physics of Bayfol HX Film Holographic Photopolymer," Polymers (Basel) **9**(12), 472 (2017).
30. J. Marín-Sáez, J. Atencia, D. Chemisana, and M.-V. Collados, "Characterization of volume holographic optical elements recorded in Bayfol HX photopolymer for solar photovoltaic applications," Opt. Express **24**(6), A720–A730 (2016).
31. J. Marín-Sáez, M. V. Collados, D. Chemisana, and J. Atencia, "Energy analysis of holographic lenses for solar concentration," Proc. SPIE **10233**, 1023317 (2017).
32. Covestro Deutschland AG, *Bayfol HX200 Datasheet* (2016).
33. P. Markovski, N. Koleva, and T. Todorov, "Some characteristics of phase holographic gratings in the intermediate regime of diffraction," Opt. Quantum Electron. **13**(6), 515–518 (1981).
34. J. Marín-Sáez, M. V. Collados, J. Atencia, and D. Chemisana, "Optical and Energetic Performance of Volume Holographic Optical Elements for Solar Energy Applications," in *Advances in Energy Research* (NOVA, 2017).
35. N. Uchida, "Calculation of diffraction efficiency in hologram gratings attenuated along the direction perpendicular to the grating vector," J. Opt. Soc. Am. **63**(3), 280 (1973).
36. M. Prijatelj, J. Klepp, Y. Tomita, and M. Fally, "Far-off-Bragg reconstruction of volume holographic gratings: A comparison of experiment and theories," Phys. Rev. A **87**(6), 63810 (2013).
37. E. Hecht, *Optics* (Addison Wesley, 1998).
38. F.-K. Bruder, F. Deuber, T. Fäcke, R. Hagen, D. Hönel, D. Jurbergs, T. Rölle, and M.-S. Weiser, "Reaction-diffusion model applied to high resolution Bayfol HX photopolymer," Proc. SPIE **7619**, 76190I (2010).

Optics EXPRESS

1. Introduction

Concentrating photovoltaics for building integration has been commonly carried out with optical refractive reflective elements [1–5]. It allows the reduction of the necessary PV cell surface while obtaining the same electrical energy. However, the concentration of the solar spectrum on the PV cell causes an increase of its temperature, which may lead to a worsening of its performance. For that reason, concentrating photovoltaics for building integration is one of the numerous fields in which the use of Holographic Optical Elements (HOEs) provides important advantages [6]. This is because the chromatic selectivity of holograms allows the concentration on the PV cell of only the spectral range of the solar radiation that will be more efficiently converted into electricity; thus avoiding wavelengths that would only contribute to overheating of the cell. If a mono-crystalline Si cell is used, with the spectral response curve shown in Fig. 1, a good design possibility would be utilizing a HOE that performs most efficiently for wavelengths around 800 nm, in order to couple the aforementioned spectral response with the solar spectrum, also plotted in Fig. 1 [7]. This wavelength will be later referred to as target wavelength.

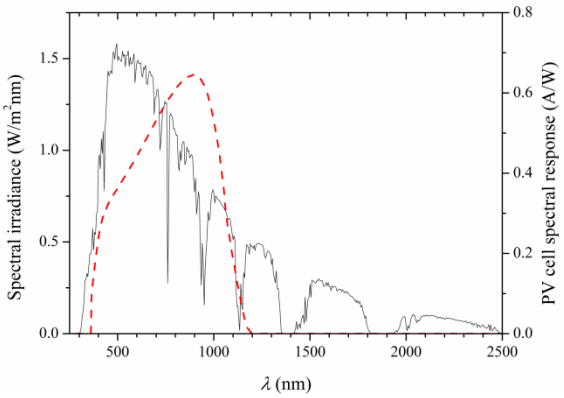

Fig. 1. Standard AM 1.5D solar spectrum [7] (solid black line, left *y*-axis). Monocrystalline Si PV cell response curve (dashed red line, right *y*-axis).

Redirection and concentration of light can be carried out either with non-concentrating HOEs (such as gratings) [8–10] or with concentrating HOEs (such as spherical or cylindrical lenses) [11–19]. Due to the angular selectivity of holograms, tracking of the apparent movement of the sun in the sky is often required in order to keep the reconstruction direction of incidence constant. However, if a holographic cylindrical lens is placed in such a way that its direction of low angular selectivity matches either the direction of solar altitude or azimuth, tracking can be suppressed in one axis [17,18].

Holograms can operate in three different regimes: the volume or Bragg regime, the transition regime, and the thin or Raman-Nath regime, depending on the recording and reconstruction conditions [20,21]. At the output of a volume hologram, i.e. a hologram operating in the volume regime, only two beams emerge: the one corresponding to the transmitted order and the one corresponding to the first order of diffraction. Under certain recording conditions and for a specific reconstruction wavelength and angle of incidence, all the energy can be transferred to the diffracted beam, thus having 100% efficiency. Volume holograms are very often used because of this characteristic.

However, volume holograms present very high chromatic selectivity. They also have high chromatic dispersion, so rays of different wavelengths emerge from the hologram with different directions and only some of them will reach the position where the PV cell would be located. These effects are accentuated the more into the volume regime the HOE performs. Although in principle they are advantages because concentration of less efficient bandwidths on the PV cell is prevented, they can be counter-productive in applications with broadband

Optics EXPRESS

spectrum reconstruction, such as solar concentration. This is because very high chromatic selectivity and dispersion involves a narrow spectral range collected by the cell, which can be narrower than its spectral sensitivity.

One way to address this issue is to multiplex [22–24], that is, to record several holograms in the same sample to enhance the wavelength acceptance. A recording material that provides very high index modulation is needed to obtain high efficiency with all the holograms [25], and the recording geometry should avoid cross-coupling among the different HOEs. To the authors' knowledge, this procedure has not been successfully carried out for solar concentration applications.

A novel approach to overcome the problem of volume holograms' high selectivity is explored in this research: the use of HOEs that operate in the transition regime for the target wavelength. This type of holograms had not been previously used in solar concentration applications. They still provide reasonably high efficiencies and have lower angular and chromatic selectivities than holograms operating further into the volume regime [26,27]. This would imply an enhancement of the spectral irradiance that is collected by the PV cell without concentrating the non-desired parts of the solar spectrum, producing higher current intensities than with volume holographic concentrators and lower cell temperatures than with refractive optical concentrators.

Three different cylindrical holographic lenses (one of them performing entirely in the volume regime for 800 nm and the other two, partly in the transition regime) were theoretical and experimentally analyzed in this study. The index modulation reached at each point of each HOE was modeled as a function of the spatial frequency and the recording exposure to include the response of the material. This was needed to solve the coupled differential equations of Coupled Wave Theory [28], which explain the behavior of HOEs.

The index modulation modeling was validated with the comparison with experimental results. Finally, the model was applied to the simulation of three holographic concentration systems with the aim of determining whether the inclusion of the transition regime is suitable for solar concentration applications.

This paper is structured as follows. The experimental recording of HOEs is described in subsection 2.1; the experimental approach carried out in this study to obtain the index modulation at each point of the HOE is explained in subsection 2.2; and the simulation of the three global systems, in subsection 2.3. The results corresponding to the determination of the index modulation are presented in subsection 3.1, the ones corresponding to the simulations of cylindrical holographic lenses and their validation with experimental recordings, in subsection 3.2, and the global system simulations, in subsection 3.3.

2. Materials and Methods

2.1. Holographic recording

The photosensitive material on which all transmission phase holograms in this work have been recorded is Bayfol HX TP photopolymer, manufactured by Covestro Deutschland AG [29]. This material had been previously tested and it was found that the needed index modulation to obtain 100% efficiency with an 800 lines/mm grating when reconstructing with 800 nm could be reached [30]. In all cases the thickness of the photopolymer layer was 16 μm. No recording materials sensitive to 800 nm exist, and since it was determined in [31] that the election of the recording wavelength did not affect significantly the resulting spectra received by the PV cell and therefore could be based on the laboratory equipment availability, the recording wavelength was 532 nm (Coherent Verdi V6 laser). The photopolymer material is laminated onto a glass slide by applying pressure, as indicated in the technical characteristics document from the manufacturers [32]. No index-matching is necessary, since the surface tension prevents the existence of air between the photopolymer and the glass. The back side of the glass slide is blackened to avoid undesired holograms recorded due to

reflections. After the recording, a two-step photocuring process with incoherent light was carried out, described elsewhere [30].

Holographic gratings were recorded with two plane waves, whereas holographic cylindrical lenses were recorded with a plane wave and a cylindrical wave. Figure 2 shows the recording setup of a cylindrical holographic lens. In order to record a grating, the cylindrical lens would be removed. Z-Direction is defined as the normal to the photopolymer plane; y-direction as parallel to its surface and is contained in the plane of incidence and x-direction is perpendicular to the plane of incidence. Parameter z_0 is the distance from the holographic plate to the focal point at 532 nm, parallel to *z*-axis.

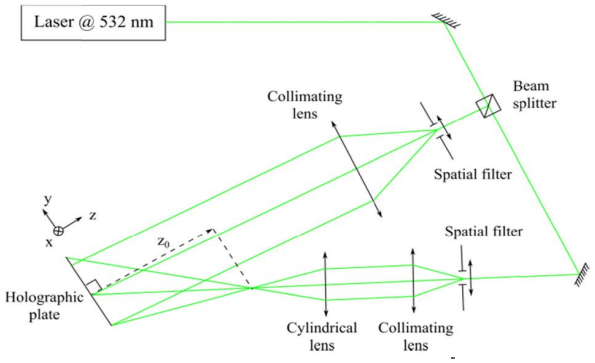

Fig. 2. Recording setup of a cylindrical holographic lens.

2.2. Experimental determination of the index modulation

The index modulation n_1 achieved during the recording of a phase hologram depends on several factors: the physical and chemical properties of the photosensitive material, the angle between beams and the recording intensity and time.

Since the angle between the recording beams of a holographic cylindrical lens is different at each position of the HOE (and thus, its spatial frequency), the index modulation reached at each point is also different. In order to find out this dependence, several slanted transmission gratings were recorded with different spatial frequencies, ranging from 70 to 1200 lines/mm. The recording intensity was kept approximately equal in all cases (around 1.4 mW/cm^2), while varying the exposure time to obtain different exposure dosages. Each hologram was then illuminated at the reconstruction stage with an 800 nm laser (ThorLabs Laser Diode CPS808A, emitting 4.4 mW) at Bragg angle and polarization perpendicular to the incidence plane.

Depending on which regime each hologram operated in for the reconstruction wavelength, the number of diffraction orders that emerged from it was different, being two for volume holograms (0 and + 1 order) and higher for holograms operating in the transition regime or the Raman-Nath regime.

The intensity of every order of diffraction that was found at the output of each hologram was measured (with Newport Power Meter Model 1815-C with detector Model 818-SL, with an uncertainty of 1 μW) and the relative efficiency of each diffraction order was calculated with

$$\eta_L = \frac{I_L}{\sum_L I_L} \tag{1}$$

where I_L is the intensity of the L diffraction order.

Optics EXPRESS

Several criteria are defined in [20] in order to determine whether a hologram operates in the volume regime: only two orders of diffraction exist (0 and + 1 orders), the efficiency of the + 1 order when Bragg condition is met is given by Kogelnik's solution [28],

$$\eta = \sin^2\left(\frac{\pi d n_1}{\lambda\sqrt{c'_{0z}c'_{+1z}}}\right) \tag{2}$$

and the efficiency of the 0 order is given by the complementary cosine function. The parameters that appear in Eq. (2) are: d, the thickness of the photopolymer layer; λ, the reconstruction wavelength and c'_{0z} and c'_{+1z}, the directional cosines inside the medium in z-direction of the transmitted and diffracted beam, respectively.

If the considered holographic grating is a volume hologram (for the reconstruction wavelength 800 nm) then the index modulation is calculated by simply substituting the efficiency in Eq. (2) when Bragg condition is met.

However, if the considered holographic grating is not a volume hologram for this wavelength, then Kogelnik's solution cannot be applied [33] and the coupled wave equations need to be solved numerically. The coupled wave equation corresponding to diffraction order L is [26,28]

$$c'_{Lz}\frac{dA_L}{dz} + j\vartheta_L A_L + j\kappa\left[A_{L+1}\left(\vec{p}_{L+1}\cdot\vec{p}_L\right) + A_{L-1}\left(\vec{p}_{L-1}\cdot\vec{p}_L\right)\right] = 0 \tag{3}$$

where A_L is the amplitude of the L order wave, c'_{Lz} is its directional cosine in z-direction, ϑ_L is the dephasing parameter, $\vec{p}_L$ is its polarization direction and κ is the coupling parameter, given by

$$\kappa = \frac{\pi n_1}{\lambda} \tag{4}$$

where the index modulation appears.

These equations were solved for each spatial frequency and for a series of index modulation values, and the value of the index modulation was determined as the one that provided diffraction efficiencies that were the closest to the previously obtained experimental ones. Afterwards, the set of index modulation data for each spatial frequency was fitted to an exponential dependency with the exposure dosage, since for exposure dosages higher than a certain value, saturation occurs. This would later allow the determination of n_1 for a specific exposure dosage.

Another aspect that affects the index modulation that can be reached, and that needs to be taken in consideration when modeling the index modulation, is the recording intensity throughout the HOE. Since laser beams present a Gaussian profile, in principle the intensity along each beam is not uniform. However, the recording beams are sufficiently expanded so that only the central part of the beams is used for the recording; therefore the intensity variation due to this effect is rather small.

When recording a holographic cylindrical lens one of the recording beams is a cylindrical beam, as shown in Fig. 2. Thus, the wavefront that reaches each point of the holographic plate is different, and so is the intensity associated with each one. Nevertheless, it has also been verified that these variations are rather small as well and correspond to a negligible change in index modulation (for the intensity and exposure dosage values later used to record holographic cylindrical lenses).

To summarize, it has been assumed that the achieved value of index modulation at each point will only be affected by the variation of spatial frequency throughout the holographic cylindrical lens.

Optics EXPRESS

2.3. Algorithm for simulations of cylindrical holographic lenses as solar concentrators

A geometrical and energetic analysis of the HOEs is carried out. A ray tracing algorithm was previously developed [34] in a MATLAB environment, which calculates the direction of propagation and the efficiency of the diffracted order in volume holograms, for any given wavelength and direction of incidence (whether or not Bragg condition is met). It can analyze both holographic gratings (in which all points behave equally) and other HOEs, such as cylindrical holographic lenses, in which the grating vector $\vec{K}$ is different at each point. Thus, each point of the holographic lenses is analyzed independently under the assumption that each one can be modeled as a distinct holographic grating ("local-grating").

This algorithm was improved so that the higher orders of diffraction that appear in non-volume holograms were considered as well. The number of diffraction orders that emerge at each point inside the medium at the reconstruction step and their direction of propagation are determined with the help of the so-called beta-value closure [26,34–36]

$$\vec{k}_L' \cdot \vec{u}_y = \left(\vec{k}_0' - L\vec{K}\right) \cdot \vec{u}_y \tag{5}$$

The y-component of the wave vector of the L order inside the medium, $\vec{k}_L' \cdot \vec{u}_y$, is given by the wave vector of the 0th order, $\vec{k}_0'$, and the grating vector $\vec{K}$. The z-component is then calculated so that the modulus of the vector $\vec{k}_L'$ is the same as that of $\vec{k}_0'$. Of course, only orders of diffraction with $\vec{k}_L' \cdot \vec{u}_y \le \left|\vec{k}_0'\right|$ are generated.

The index modulation of each point was assigned by means of its dependence with the spatial frequency determined in subsection 3.1. Then the efficiency of each order of diffraction was calculated by a numerical resolution of the coupled wave equations (as explained in subsection 2.2) for each point of the HOEs and each reconstruction wavelength and angle of incidence.

The system in Fig. 3, previously proposed in [19], is considered in this study. It comprises two identical and symmetrically placed cylindrical holographic lenses that redirect sunrays to a mono-crystalline Si PV cell. Sunlight that goes through the space between the HOEs also reaches the PV cell. It can easily be integrated on a building façade by superimposing it on the blinds of a solar louvre shading system, which tracks the solar altitude by rotating around *x*-axis.

When carrying out simulations of this specific system, the standard AM 1.5D solar spectrum is considered. Since sunlight is unpolarized the coupled wave equations are solved for two polarizations (parallel and perpendicular to the incidence plane), and the final efficiency of each ray and each wavelength is the average of the ones corresponding to each polarization. Fresnel reflection losses [37], which are different for each polarization, are also taken into account. The irradiance that is found at the surface of the PV cell, placed at a specific location, is calculated by integrating the power associated with each ray that reaches it and dividing by the surface. The product of the spectral irradiance and the spectral response of the PV cell gives the peak current intensity that is generated by the PV cell, when no temperature effects are considered. These procedures are explained in detail in a previous publication [34].

Optics EXPRESS

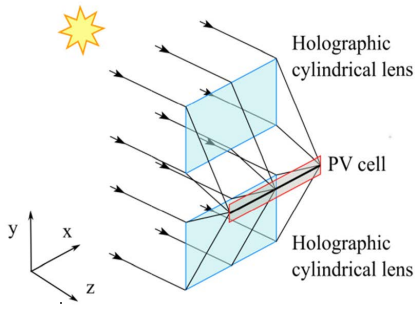

Fig. 3. Schematic of the system considered: each cylindrical holographic lens redirects sun rays towards a PV cell.

The *y*- and *z*-position of the PV cell for each specific system (and therefore, the *y*-distance between the two HOEs) is optimized with the following criteria:

- When reconstructing with perpendicular incidence all rays corresponding to the + 1 order of diffraction and 800 nm must reach the PV cell. Moreover, none of the rays of the 0 order of diffraction should reach it, in order to avoid the incidence of infrared.
- The current intensity generated by the PV cell when reconstructing with the range of the solar spectrum optimum for its coupling with the PV cell (in this work, 700-900 nm) must be maximal.

3. Results and Discussion

3.1 Determination of the index modulation

Several slanted gratings with spatial frequencies within 70-1200 lines/mm were recorded on Bayfol HX photopolymer with the same recording intensity and different exposure dosages, as explained in subsection 2.2. Table 1 shows the angle between the recording beams and the spatial frequency of each grating. When reconstructing at 800 nm a different number of diffraction orders were found at the output of the gratings, as indicated in Table 1. The appearance of higher orders of diffraction and the observed distribution of intensity among them clearly illustrates the gradual shift from Bragg regime to the transition regime and to Raman-Nath regime, also stated in Table 1.

Table 1. Characteristics of the recorded holographic gratings.

$\Delta\theta_{recording,\,air}$ (°)	SF (lines/mm)	Number of diffraction orders @ 800 nm	Regime @ 800 nm
37.2	1199	2	Volume
30.9	1001	2	Volume
25.0	814	2	Volume
19.0	620	2	Volume
15.5	507	4	Transition
12.5	409	4	Transition
9.0	295	4	Transition
6.0	197	6	Transition
3.0	98	9	Transition
2.1	70	9	Thin

The index modulation (calculated as described in subsection 2.2) obtained for each grating when varying the recording time, and thus, the exposure dosage, is plotted with markers in Fig. 4.

Optics EXPRESS

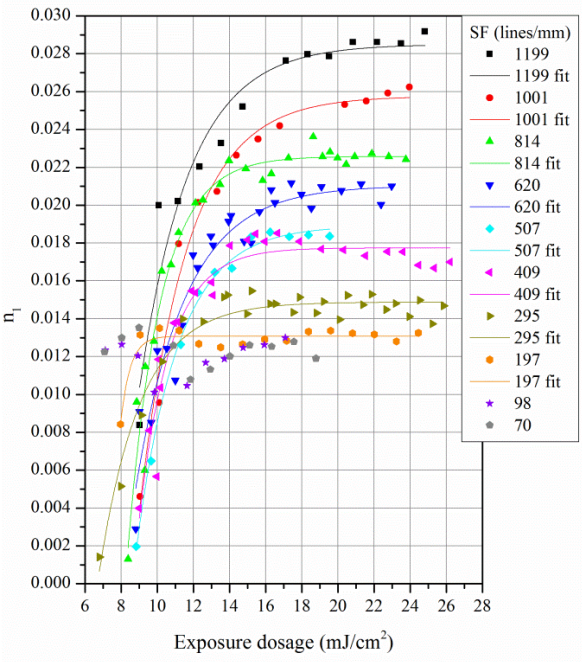

Fig. 4. Index modulation experimental values as a function of the exposure dosage for several spatial frequencies.

The index modulation obtained with each spatial frequency (using the same recording intensity) for a certain exposure dosage is different, and it decreases with the angle between the recording beams. This is in agreement with other studies on photopolymers for holographic recording [38]. Therefore, it cannot be assumed that the index modulation achieved at each point of a holographic lens with spatial frequencies varying in the range shown in Fig. 4 is the same.

Each set of index modulation data for a given spatial frequency is fitted to an exponential dependency with the exposure dosage. The resulting index modulation values at 16 mJ/cm^2 are plotted in Fig. 5. This exposure dosage was selected because it would later be used to record the cylindrical holographic lenses. It shows a linear dependency, $n_1 = (1.31 \pm 0.04) \cdot 10^{-5} SF + (0.0114 \pm 0.0003)$, where the spatial frequency, SF, is expressed in lines/mm. This allows the estimation of the index modulation at each point of a holographic lens recorded with this exposure dosage.

3.2 Experimental validation of the index modulation modeling with cylindrical holographic lenses

Three holographic cylindrical lenses (later referred to as A, B and C) were considered, each with a different range of spatial frequencies, shown in Fig. 6. The white, light grey and dark grey areas denote Bragg, transition and Raman-Nath regimes, respectively, when reconstructing the designed lenses (with the calculated index modulations) with 800 nm. All points in lens A operate in Bragg regime for this wavelength, roughly two thirds of the points in lens B (with $y \leq 10$ mm approximately) operate in Bragg regime and the rest in the transition regime, and roughly one third of the points in lens C (with $y \leq -10$ mm approximately) operate in Bragg regime, with the rest operating in the transition regime except for the point with $y = 25$ mm, which operates in Raman-Nath regime.

Optics EXPRESS

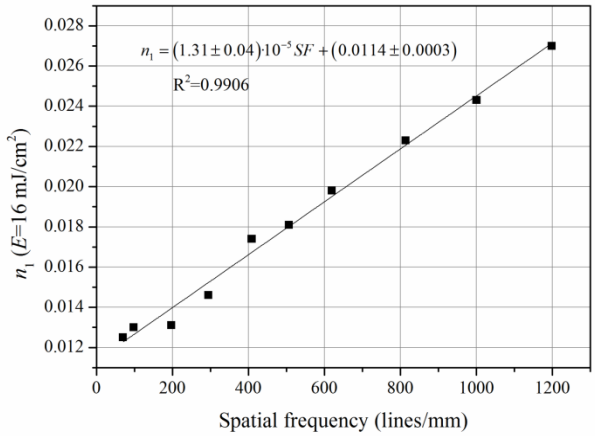

Fig. 5. Linear fit of the obtained values of the index modulation with a recording exposure dosage of 16 mJ/cm^2 versus the spatial frequency.

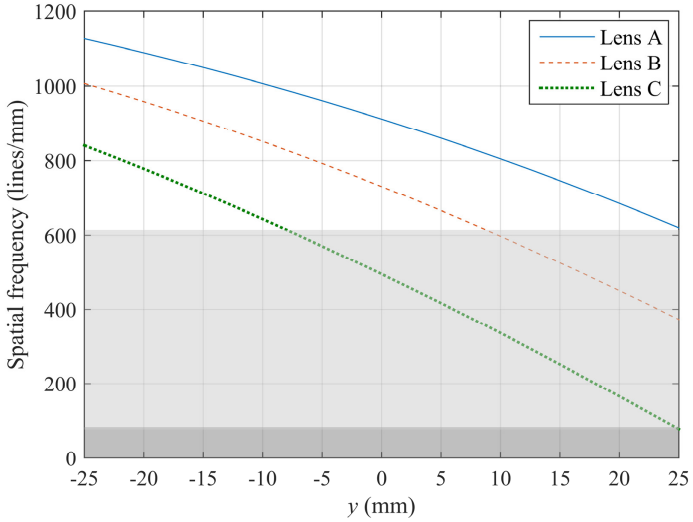

Fig. 6. Spatial frequency along y-direction of all three lenses. The white, light grey and dark grey areas denote Bragg, transition and Raman-Nath regime, respectively, when reconstructing with 800 nm.

The recording angles are presented in Table 2, where θ_p is the angle of the plane wave and $\theta_{c,center}$ is the angle of the cylindrical wave at the center of the hologram, in air. These angles ensured that Bragg condition was met at the center of the lens when illuminating with 800 nm and perpendicular incidence at the reconstruction stage. The angle of the recording plane waves is not zero because of the difference between the recording and the target wavelength. The distance from the holographic plate to the focal point at 532 nm, parallel to z-axis, marked as z_0 in Fig. 2, is the same for all three lenses, 105 mm. This provides a focal point at 800 nm that is 70 mm away from the holographic plate, measured in the direction of z-axis.

Optics EXPRESS

Table 2. Recording angles of the three cylindrical holographic lenses considered

	Lens A	Lens B	Lens C
θ_p (°)	7.2	5.7	3.8
$\theta_{c,center}$ (°)	36.5	28.7	19.1

The diameter of the recorded holographic lenses was slightly bigger than 50 mm. The exposure dosage at the center of all lenses was 16 mJ/cm^2, which provides the necessary index modulation to obtain 100% efficiency at the center of lens A when reconstructing perpendicularly with 800 nm.

After the recording and photocuring, all three HOEs were reconstructed with an 800 nm laser beam (with an approximate diameter of 0.5 mm and perpendicular polarization, with the model specified in the previous subsection) that illuminated with normal incidence a point of the HOE, every 2.5 mm. The intensity of each detectable diffraction order was measured and the efficiency was calculated with Eq. (1) as explained in subsection 2.2. The experimental data are plotted in Fig. 7 with filled circles of various colors (each color corresponds to a different order of diffraction). The solid lines are the theoretical curves obtained by numerically solving the coupled wave equations, with index modulation values assigned to each point based on Fig. 5, as detailed in subsections 2.2 and 2.3. A good agreement between the experimental and theoretical results is observed, validating the index modulation determination throughout the lenses.

The number of diffraction orders that appear at the output of each lens is consistent with the expected operating regimes in Fig. 6: only two in the volume regime and more in the rest. At y = 25 mm of Lens C, the theoretical and experimental efficiencies of the diffraction orders pairs + 1 and −1, and + 2 and −2 are nearly the same, corroborating the operation in Raman-Nath regime.

When reconstructing perpendicularly at 800 nm only the central points of each lens with y = 0 mm fulfill Bragg condition, since the recording wavelength was 532 nm. However, only the central point of lens A reaches 100%, not the one of lens B or C. This is because the index modulation achieved at y = 0 mm in lens A is the one that provides 100% efficiency for its spatial frequency when reconstructing with 800 nm at perpendicular incidence. Although Bragg condition is also met with that wavelength and angle of incidence at the central point of the other two lenses, the index modulation needed to obtain 100% efficiency is different from the one reached with the recording intensity and exposure dosage considered.

When moving away from the center of the lenses towards negative y, the efficiency of the + 1 diffraction order decreases faster than towards y positive, as expected due to the higher angular selectivity of HOEs with higher spatial frequency and therefore, that are deeper into the volume regime.

3.3 Simulations of cylindrical holographic lenses as solar photovoltaic concentrators

Three global systems (systems A, B and C) like the one represented in Fig. 3 were considered. Each one comprises two identical cylindrical holographic lenses (lenses A, B or C) with index modulations calculated in subsection 3.1 corresponding to a recording exposure dosage of 16 mJ/cm^2. They are placed in a symmetrical configuration so that they redirect sunrays impacting with perpendicular incidence towards the same PV cell: a mono-crystalline Si PV cell, with the spectral response curve of Fig. 1. Its y-dimension is 10 mm and the x-dimension is the same as the HOE's. The space between the two HOEs allows sunrays to go through and reach the PV cell, so the geometrical concentration of the global system is x11. This configuration was explored in a previous publication [19] and can easily be integrated on a building façade. The position of the PV cell was optimized with the criteria explained in subsection 2.3, and the coordinates are given in Table 3 (the center of the lower holographic lens has coordinates y = 0 mm, z = 0 mm in all three cases).

Optics EXPRESS

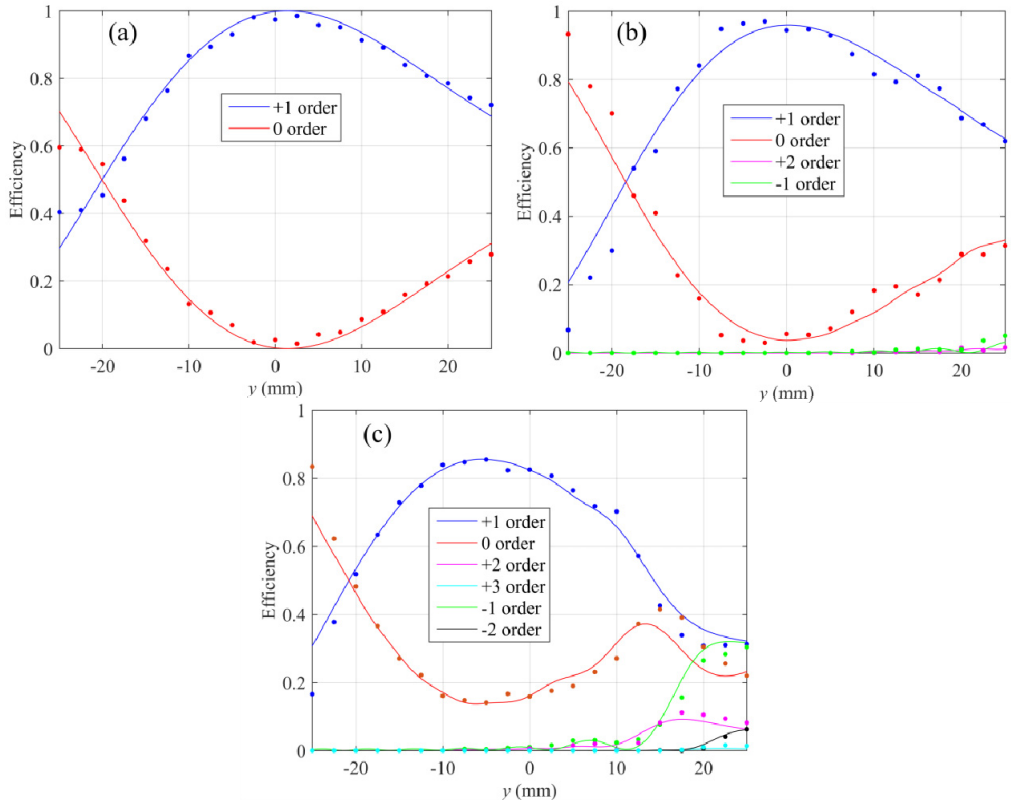

Fig. 7. Experimental (filled circles) and theoretical (solid lines) efficiencies of each order of diffraction found at the output of cylindrical holographic lenses A (a), B (b) and C (c).

Table 3. Position of the PV cell and current concentration coefficients for each one of the three systems considered.

	Lens A	Lens B	Lens C
z_{cell} (mm)	40	52	68
$y_{cell,\,center}$ (mm)	44	38	30
$CC_{current,\,1\,HOE}$	0.61	1.01	1.36
$CC_{current,\,global\,sist}$	2.22	3.02	3.72

Simulations of the three global systems were carried out when reconstructing with perpendicular incidence. In order to obtain results as realistic as possible, the unpolarized standard AM 1.5D solar spectrum [2] was considered, as well as reflection Fresnel losses in all three interfaces (air-photopolymer, photopolymer-substrate, substrate-air).

The spectral irradiance received by the whole surface of the PV cell with only one of the two lenses of systems A, B and C is plotted in Fig. 8. The different colors correspond to different orders of diffraction that reach the PV cell (diffraction orders 0, −1 and −2 of all lenses and order + 3 of lens A do not reach it and are not included in the graphs). The standard AM 1.5D solar spectrum [7] and spectral response curve of the mono-crystalline Si PV cell from Fig. 1 have been included in the graph for comparison. In all three cases the received spectrum comprises wavelengths around 800 nm, as expected, so the solar spectrum is enhanced in a range that the PV cell performs more efficiently.

Optics EXPRESS

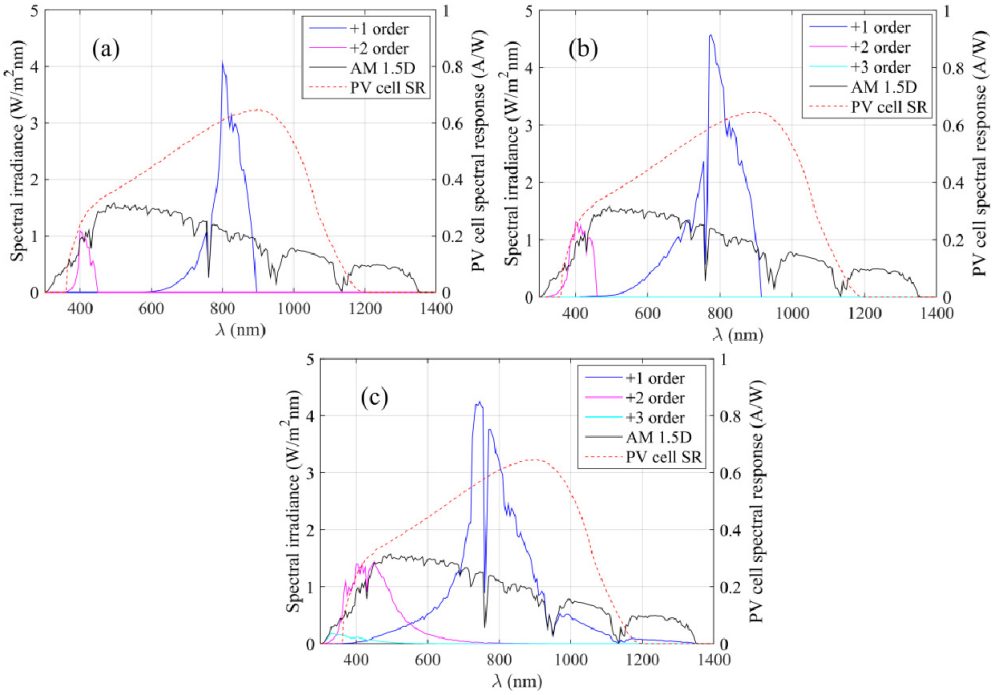

Fig. 8. Spectral irradiance received by the PV cell with lens A (a), B (b) and C (c) (colored solid lines, left *y*-axis). Only orders of diffraction that reach the PV cell are included. Standard AM 1.5D solar spectrum [7] (black solid line, left *y*-axis), and mono-crystalline Si PV cell spectral response curve (red dashed line, right *y*-axis) included for comparison.

It is clearly observed in Fig. 8 that the received spectrum corresponding to the + 1 order of diffraction belongs to a broader spectrum for lens C than lens B and than lens A. In other words, the more into the transition regime the lens operates; a broader irradiance spectrum is collected by the PV cell. This is due to the lower chromatic selectivity and dispersion of HOEs in the transition regime: more rays and with higher energy reach the PV cell.

Besides, when the transition regime is included, higher orders of diffraction (+ 2 in lens A and + 2 and + 3 in lenses B and C) reach the PV cell. Despite the fact that lens A operates entirely in the volume regime at 800 nm, when the reconstruction wavelength is shorter part of the lens operates in the transition regime, so higher orders of diffraction appear. Likewise, order + 3 emerges lens B with shorter reconstruction wavelengths, although its irradiance at the PV cell is negligible. The spectral ranges of orders + 2 and + 3 at the cell in all cases correspond to wavelengths around 400 nm, which the PV cell will also transform into electrical current, although with a lower response than that of the optimal range. The irradiance associated with order + 2 with lens C is higher than that of lenses A and B, illustrating its lower chromatic selectivity and dispersion.

The maximal spectral irradiance received with lens A is found at 800 nm, as expected. However, that is not the case with lens B or C. This is due to the index modulation reached at each point of the lenses. As mentioned in the previous subsection, the recording exposure dosage (and therefore, the index modulation) was optimized for 800 nm only for lens A, and then the same recording intensities and exposure dosages were used for lens B and C. Then the efficiency of 800 nm rays exiting the HOEs is lower than that of rays with wavelengths slightly shorter than 800 nm, and due to the lower chromatic dispersion most of them reach the PV cell as well.

The results in Fig. 8 confirm that these HOEs do not concentrate the infrared part of the solar spectrum that the PV cell cannot use: there is a cutoff in the received irradiance in Figs.

8(a) and 8(b) at approximately 900 nm, and lens C (Fig. 8(c)) only redirects towards the cell a negligible percentage of the solar irradiance of wavelengths longer than 1100 nm. The ray tracing analysis has demonstrated that due to several effects (chromatic dispersion, total internal reflection and the nonexistence of the + 1 diffracted order for long wavelengths) no irradiance with wavelengths longer than 1400 nm reaches the cell. Thus, the increase of the cell temperature would be reduced, so that it would not cause a worsening of its performance.

In order to calculate the spectral irradiance when considering the whole system, the curves in Fig. 8 have to be doubled, since both lenses in each system are identical and symmetrically placed, and the solar spectrum from Fig. 1 needs to be added, which corresponds to light that goes through the space between the lenses. Although this means that the PV cell will receive infrared radiation that it cannot convert into electricity, it will not be concentrated, unlike with refractive concentrating elements, and therefore, the increase in temperature will be rather low. The maximal optical efficiency obtained with system A is 76%; with system B, 79% and with system C, 72%.

The generated current intensity depends on the irradiance associated with each wavelength, as indicated by the spectral response curve of the mono-crystalline Si cell of Fig. 1. The current concentration coefficient, $CC_{current}$, defined in [34], is the ratio between the total current intensity obtained with the holographic concentrator and the current intensity that would be obtained without the HOE. The resulting values when considering one lens of each system, $CC_{current,1\,HOE}$, and the whole system, $CC_{current,\,global\,syst}$, are included in Table 3. They demonstrate the advantage of using HOEs operating in the transition regime rather than the volume regime for the target wavelength in solar concentration applications, since the current concentration obtained with lens C, 1.36, doubles the value with lens A and is also higher than the one with lens B. Although these values may seem low, it has to be remembered that it is not the whole solar spectrum what is being concentrated, but a small range of it, which corresponds to the most efficient spectral range that the chosen PV cell can transform into electricity, without being affected by temperature effects.

Another aspect that needs to be analyzed is the spatial distribution of the irradiance received by the cell, or more precisely, of the current generated. Due to the chromatic dispersion of holograms the spectral irradiance received at each point of the cell is different, which causes the peak current intensity at each point to be different as well. The current intensity should be as homogeneous as possible throughout the cell, since the lowest value will limit the resulting current intensity.

Figure 9 shows the current concentration coefficient along *y*-dimension of the PV cell with one lens of each system (a) and with each whole system (b). Although the variations of this coefficient for lens A and B are relatively small, the current distribution for lens C is rather inhomogeneous. Nevertheless, this problem is reduced when considering the whole system C, since the part of the PV cell with lower current concentration due to one HOE would correspond to higher current concentration due to the other HOE, and vice versa, and the resulting current concentration is more homogeneous.

These simulations have been carried out for perpendicular incidence only, that is, with two-axes tracking. However, this system would only track the solar altitude movement [19], so the azimuth angle variation along the day would correspond to the direction of low angular selectivity of the HOEs (which in Fig. 3 corresponds to directions of incidence contained in plane *XZ*). Except at solar midday, incidence will not be perpendicular and this will cause a change in the direction of the output rays, not reaching the PV cell. The use of HOEs operating in the transition regime is also advantageous when considering this effect, since this change is smaller, and because they have lower angular selectivity.

Optics EXPRESS

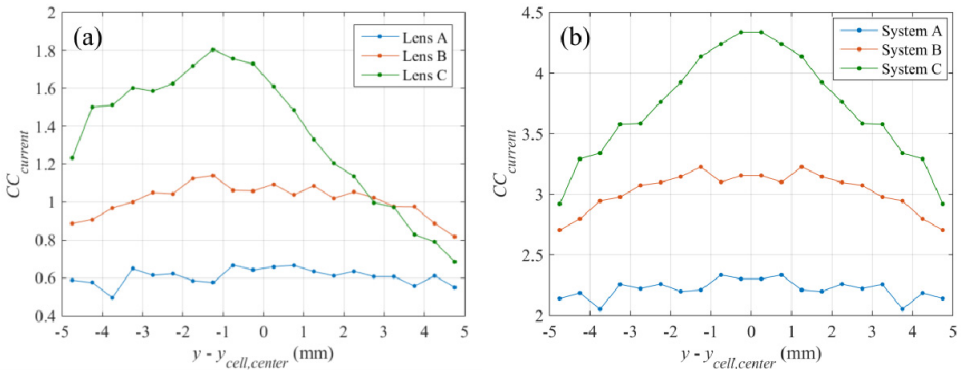

Fig. 9. Current intensity concentration throughout the PV cell with one lens (a) and with the whole system (b) A (blue curve), B (orange curve) and C (green curve).

4. Conclusions

This study focuses on HOEs partly operating in the transition regime between the Bragg and Raman-Nath regimes with the scope of analyzing the performance of cylindrical holographic lenses for solar concentration for building integration. This is a novel approach that, to our knowledge, had not been considered in broadband reconstruction spectrum applications. The change in index modulation throughout the HOEs due to the variation of the spatial frequency has been considered, in order to include the material's response. The index modulation of gratings recorded in Bayfol HX photopolymer with various spatial frequencies was determined, revealing a linear dependence for the recording intensity and exposure utilized. The index modulation values were needed to solve the coupled differential equations corresponding to each point of three different holographic lenses operating in the transition regime, where Kogelnik's solution [28] cannot be applied.

Future work must include experimental tests of the PV cell with these holographic concentrators and a study of the temperature of the cell.

Funding

Generalitat de Catalunya (2017FI_B2_00127); Ministerio de Economía y Competitividad of Spain (ENE2013-48325-R, ENE2016-81040-R); Diputación General de Aragón - Fondo Social Europeo (TOL research group, T76); Universidad de Zaragoza (UZ2017-CIE-02).

Acknowledgements

The authors would like to thank Dr. Enrico Orselli (Covestro Deutschland AG) for supplying the recording photopolymer material.